

## Nonlinear optical response of two-dimensional magnetoexcitons

Charles Stafford\* and Stefan Schmitt-Rink  
AT&T Bell Laboratories, Murray Hill, New Jersey 07974

Wilfried Schaefer  
Forschungszentrum Jülich, 5170 Jülich, West Germany  
(Received 16 January 1990)

We study the nonlinear optical response of two-dimensional excitons in a perpendicular magnetic field. The transition from two-dimensional behavior in low fields to quasi-zero-dimensional behavior in high fields is investigated, and pronounced interaction effects that are highly field dependent are found. Differential pump-probe spectra are calculated for both continuous-wave and impulsive excitation. It is shown that cyclotron motion can be time resolved with ultrashort optical pulses.

### I. INTRODUCTION

Over the past several years, semiconductor nanostructures have attracted much attention because of their novel optical and transport properties. For example, it is now well established that confinement of excitons on length scales smaller than the bulk Bohr radius leads to an enhanced resonant optical response. Here, in addition to quasi-two-dimensional quantum wells,<sup>1</sup> quasi-zero-dimensional quantum dots have been of interest recently.<sup>2-9</sup> One of the important questions is the dependence of nonlinear optical effects on quantum confinement. In this paper, we address this issue in the context of two-dimensional (2D) excitons in a perpendicular magnetic field.<sup>10-17</sup> For strong fields, this system shares many features with other quasi-zero-dimensional systems, such as semiconductor microcrystallites. Experimentally, it provides a very controlled environment to study the intrinsic physics of three-dimensional (3D) quantum confinement. Naturally, 2D magnetoexcitons are also of interest in their own right.

### II. LINEAR OPTICAL RESPONSE

The linear optical properties of 2D magnetoexcitons were discussed many years ago by Akimoto and Hasegawa<sup>10</sup> and Shinada and Tanaka.<sup>11</sup> In the presence of a perpendicular magnetic field  $\mathbf{H}=(0,0,H)$  and within the effective-mass approximation, the Wannier equation for a 2D electron-hole ( $e-h$ ) pair with zero center-of-mass momentum reads (omitting the band gap and Zeeman energies)

$$\left[ \frac{1}{2m_e} \left( \mathbf{p} + \frac{e}{2c} \mathbf{H} \times \mathbf{r} \right)^2 + \frac{1}{2m_h} \left( \mathbf{p} - \frac{e}{2c} \mathbf{H} \times \mathbf{r} \right)^2 - \frac{e^2}{\epsilon_0 r} \right] \phi_\alpha(\mathbf{r}) = E_\alpha \phi_\alpha(\mathbf{r}), \quad (1)$$

where all symbols have their usual meaning. For  $H=0$ , Eq. (1) has a 2D hydrogenic spectrum, composed of

discrete (bound-state) and continuous (scattering-state) parts.<sup>18</sup> For  $H \neq 0$ , the spectrum is always discrete, because the effective potential

$$V_{\text{eff}}(r) = -\frac{e^2}{\epsilon_0 r} + \frac{e^2 H^2 r^2}{8mc^2} \quad (2)$$

is infinitely high. Here,  $m$  is the reduced  $e-h$  mass,  $m^{-1} = m_e^{-1} + m_h^{-1}$ . It follows immediately that all  $H \neq 0$   $e-h$  pair states must extrapolate to bound  $e-h$  pair states at  $H=0$ .<sup>10,11</sup>

The strength of the  $e-h$  Coulomb interaction may be characterized by the 3D Rydberg  $E_0 = me^4/2\epsilon_0^2$  and Bohr radius  $a_0 = \epsilon_0/me^2$ , and that of the magnetic field by the  $e-h$  cyclotron frequency  $\omega_c = eH/mc$  and magnetic length  $l = (c/eH)^{1/2}$  (throughout the article  $\hbar=1$  is used). The dimensionless parameter traditionally used to describe the relative importance of these two energy and length scales is  $\lambda = (a_0/l)^2 = \omega_c/2E_0$ , i.e., the ratio of magnetic and Coulombic zero-point energies.

The Wannier equation (1) has been previously solved by Wentzel-Kramers-Brillouin (WKB) methods,<sup>10</sup> numerical integration,<sup>11</sup> and Padé approximants based on perturbation expansions about the weak- and strong-field limits.<sup>12</sup> We followed the latter approach and expanded the  $e-h$  pair wave functions  $\phi_\alpha(\mathbf{r})$  in terms of Landau orbitals  $\phi_{nm}(\mathbf{r})$ , i.e., the solutions of Eq. (1) in the absence of  $e-h$  Coulomb interaction. This choice of a strong field or uncorrelated  $e-h$  pair basis was also encouraged by statements in the literature that for  $\lambda > 1$  a few [ $O(10)$ ] Landau levels should suffice to solve Eq. (1) with about 10% accuracy.<sup>17</sup> Here,  $n$  is the Landau-level index,  $m$  the azimuthal quantum number, and  $E_{nm}/E_0 = \lambda(2n-1)$ . For optically active  $s$ -like excitons, one readily finds for the expansion coefficients (omitting the index  $m=0$ ) (Ref. 12)

$$\sum_{n'} [\lambda(2n-1)\delta_{n,n'} - V_{n,n'}] \phi_\alpha(n') = E_\alpha \phi_\alpha(n), \quad (3)$$

where ( $n \leq n'$ )

$$V_{n,n'} = \left( \frac{2\lambda}{\pi} \right)^{1/2} \frac{\Gamma(n'-n+\frac{1}{2})\Gamma(n-\frac{1}{2})}{\Gamma(n'-n+1)\Gamma(n)} \times {}_3F_2 \left[ \begin{matrix} 1-n, n'-n+\frac{1}{2}, \frac{1}{2} \\ n'-n+1, \frac{3}{2}-n \end{matrix} ; 1 \right]. \quad (4)$$

Here and in the following, energies and lengths are measured in units of  $E_0$  and  $a_0$ , respectively. [Equation (3) may of course also be derived by expanding the  $e$ - $h$  pair wave functions into  $e$  and  $h$  Landau-level product states and noting that optical transitions only take place between Landau levels with the same index  $n$ .]

We diagonalized Eq. (3) using standard EISPACK routines for basis sets up to 1700 Landau orbitals. Figure 1 shows the energy of the  $1s$  exciton as a function of  $\lambda$ . The dashed line is the exact result taken from Refs. 11 and 12; the solid lines show the diagonalization results for basis sets of various sizes (20, 60, and 500 Landau orbitals). Due to the truncation, our results for small  $\lambda$  always scale like  $-\lambda^{1/2}$  [i.e., like the  $e$ - $h$  Coulomb interaction equation (4)], while the exact result including the diamagnetic shift is  $E_{1s} = -4 + 3\lambda^2/32$ . The smaller the basis set, the more pronounced this artificial behavior. For  $\lambda \sim 1$ , reasonable agreement with the exact result may be achieved by considering  $O(10^2)$  basis states.

The qualitative behavior of the  $1s$  exciton energy as a function of  $l$  is essentially the same as that in a quantum dot, e.g., a planar square box of width  $l$ .<sup>19</sup> With decreasing  $l$ , the  $e$  and  $h$  come closer together and hence their potential energy increases in magnitude (as  $1/l$  for small  $l$ ). However, the zero-point kinetic energy due to quantum confinement increases faster (as  $1/l^2$  for small  $l$ ), which results in a monotonically increasing  $1s$  exciton energy. For small  $l$ , the  $e$  and  $h$  are essentially in the lowest Landau orbital and the  $1s$  exciton energy is given by  $E_{1s} = \lambda - (2\pi\lambda)^{1/2}$ .

Unfortunately, the energy of the  $1s$  exciton is not a

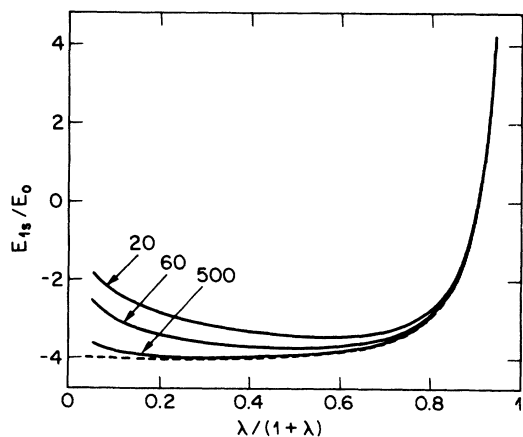


FIG. 1. Energy of the  $1s$  exciton in 3D Rydbergs as a function of magnetic field [ $\lambda = (a_0/l)^2$ , where  $l$  is the magnetic length and  $a_0$  the 3D Bohr radius]. Dashed lines: exact result taken from Refs. 11 and 12. Solid lines: diagonalization results for basis sets of 20, 60, and 500 Landau orbitals.

good measure of the size of the basis set required to describe optical spectra. Including a phenomenological transverse relaxation rate  $\gamma_2$ , the linear optical susceptibility for a given  $e$ - $h$  spin configuration reads<sup>10,11</sup>

$$\chi^{(1)}(\omega) = \frac{\lambda}{2\pi} \sum_{\alpha} \frac{|\mu \sum_n \phi_{\alpha}(n)|^2}{E_{\alpha} - \omega - i\gamma_2}, \quad (5)$$

where  $\mu$  is the interband dipole matrix element and  $\lambda/2\pi$  the Landau-level degeneracy. Figure 2 shows the imaginary part of  $\chi^{(1)}(\omega)$  for various magnetic fields,  $\gamma_2 = 0.7$  and  $|\mu|^2 = 1$ , calculated with a basis set of 1700 Landau orbitals. The spectra clearly display the transition from 2D behavior<sup>18</sup> to the discrete absorption spectrum characteristic of quasi-zero-dimensional systems; in particular, the monotonic increase in exciton oscillator strength due to quantum confinement.<sup>10,11</sup> However, they also contain a liability. Although one might expect that 1700 Landau orbitals should be sufficient for the smallest magnetic field considered by us [ $\lambda = 0.25$ , Fig. 2(a)], the corresponding  $1s$  exciton oscillator strength is about 10% smaller than that in zero field.<sup>18</sup> (Because of the decrease in  $e$ - $h$  separation, the exact result is slightly larger.<sup>11</sup>) For 500 Landau orbitals, which for  $\lambda = 0.25$  give the  $1s$  exciton energy with about 5% accuracy, the error in the  $1s$  exciton oscillator strength would be about 40%. The expansion in terms of Landau orbitals thus converges very slowly. The origin of this behavior is the fact that Landau levels are equidistant. In this (technical) respect, the situation is different from that in quantum dots, where the energy of uncorrelated  $e$ - $h$  pairs increases quadratically with quantum number and significantly

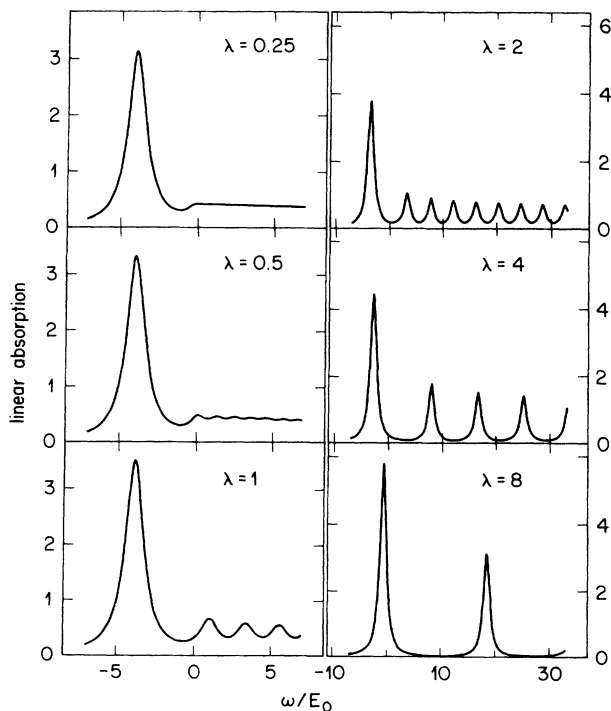


FIG. 2. Linear absorption spectra for various magnetic fields, calculated with a basis set of 1700 Landau orbitals. (a)  $\lambda = 0.25$ , (b)  $\lambda = 0.5$ , (c)  $\lambda = 1$ , (d)  $\lambda = 2$ , (e)  $\lambda = 4$ , (f)  $\lambda = 8$ .

fewer basis states are required.<sup>8</sup>

Even for the largest field considered by us [ $\lambda=8$ , Fig. 2(f)] the  $1s$  exciton oscillator strength still differs by a factor of about 3 from its asymptotic uncorrelated  $e$ - $h$  pair value  $\lambda/2\pi$ . (In the case of GaAs quantum wells and with pulsed magnetic fields, values of  $\lambda$  around 10 are the maximum attainable.) This persistence of significant inter Landau-level  $e$ - $h$  Coulomb interactions leads to interesting nonlinear optical effects that we will now discuss.

### III. NONLINEAR OPTICAL RESPONSE

Excitonic optical nonlinearities originate from exciton-exciton interactions and anharmonicities in the exciton-photon and exciton-phonon interactions. Here, we will limit ourselves to nonlinear optical effects due to anharmonic exciton-photon and exciton-exciton interactions and describe relaxation processes in the usual phenomenological fashion. Although this simplifies the situation considerably, it still leaves us with an unsolvable problem, because the determination of the  $(2n-1)$ st-order nonlinear optical susceptibility  $\chi^{(2n-1)}$  requires the exact knowledge of *all* possible states of up to  $n$   $e$ - $h$  pairs (excitons, biexcitons, triexcitons, etc.). Recently, there have been first calculations along these lines,<sup>8,20</sup> resulting in an essentially exact determination of  $\chi^{(3)}$  for semiconductor microcrystallites.<sup>8</sup> Unfortunately, because of the large size of the basis set required to describe just the single  $e$ - $h$  pair states, we cannot follow this approach here, but have to introduce one further approximation, namely the factorization of multiple  $e$ - $h$  pair states into products of single  $e$ - $h$  pair ones. This is of course nothing but the unrestricted Hartree-Fock (HF) approximation introduced earlier by Schmitt-Rink, Chemla, and Haug<sup>21,22</sup> and rederived many times.<sup>23-25</sup> Conceptually, this approach is a straightforward extension of Anderson's theory of collective excitations in superconductors<sup>26</sup> to (i) the particle-hole channel and (ii) open systems, and leads to Ginzburg-Landau-like equations for the third-order nonlinear optical response.

(Unrestricted) HF theories have some tradition in the context of 2D Coulomb systems in perpendicular magnetic fields, because they become exact in the strong-field limit (in the case of one-component plasmas, for integral filling factor only).<sup>13-16</sup> For example, in thermal equilibrium and for  $(l/a_0) \rightarrow 0$ , they yield the remarkable (and exact) result that an ensemble of spin-polarized  $1s$  magnetoexcitons behaves like an ideal (i.e., noninteracting) Bose gas, due to *local* charge neutrality.<sup>13,14</sup> This is of course only true as long as virtual excitations to excited states can be neglected. As shown recently for quantum dots,<sup>8,27</sup> the latter may reintroduce bound biexcitons, at least in unpolarized systems.

Later, we will discuss the third-order nonlinear optical susceptibility  $\chi^{(3)}$  as measured in pump-probe experiments with circularly polarized light of a given orientation. Due to the spin polarization of excitons, the formation of bound biexcitons is then impossible and the unrestricted HF theory captures most of the important physics. In addition, we may continue to ignore the Zeeman terms (as in the preceding section), because they only

shift the zero of energy.

The unrestricted HF theory treats on equal footing the effects of the laser field and the Coulomb interaction. Within the rotating-wave approximation, the equal-time density matrix projected onto  $e$  and  $h$  Landau orbitals satisfies the Liouville equation<sup>21,22</sup>

$$\left. \frac{\partial}{\partial t} \hat{n}_n(t) = -i[\hat{\epsilon}_n(t), \hat{n}_n(t)] + \frac{\partial}{\partial t} \hat{n}_n(t) \right|_{\text{relax}}, \quad (6)$$

where

$$\hat{n}_n(t) = \begin{pmatrix} n_{cn}(t) & \psi_n(t) \\ \psi_n^*(t) & n_{vn}(t) \end{pmatrix} \quad (7)$$

and

$$\hat{\epsilon}_n(t) = \begin{pmatrix} \epsilon_{cn} & -\mu E(t) \\ -\mu^* E^*(t) & \epsilon_{vn} \end{pmatrix} - \sum_{n'} V_{n,n'} \hat{n}_{n'}(t). \quad (8)$$

Here,  $\epsilon_{cn} = (2n-1)\lambda m/m_e$  and

$$\epsilon_{vn} = -(2n-1)\lambda m/m_h + \sum_{n'} V_{n,n'}$$

are the conduction- ( $c$ ) and valence- ( $v$ ) electron energies and  $n_{cn}$  and  $n_{vn}$  the respective distributions.  $\psi_n$  is the  $e$ - $h$  pair amplitude induced by the laser field  $E(t)$ , related to the total induced polarization through

$$P(t) = \frac{\lambda \mu^*}{2\pi} \sum_n \psi_n(t). \quad (9)$$

Were it not for the second term in Eq. (8), Eqs. (6)–(9) would be identical to the optical Bloch equations for an inhomogeneously broadened two-level atom. The Coulomb interaction modifies this picture in two ways: (i) the  $e$ - $e$  and  $h$ - $h$  Coulomb repulsions renormalize the individual  $e$  and  $h$  energies [diagonal elements in Eq. (8)],

$$\epsilon_{in} \rightarrow \epsilon_{in} - \sum_{n'} V_{n,n'} n_{in'}(t), \quad i=c,v \quad (10)$$

and (ii) the  $e$ - $h$  Coulomb attraction renormalizes the Rabi frequency at resonance [off-diagonal elements in Eq. (8)]

$$\mu E(t) \rightarrow \mu E(t) + \sum_{n'} V_{n,n'} \psi_{n'}(t). \quad (11)$$

Both changes express the fact that in the presence of Coulomb interactions an  $e$ - $h$  pair in a given Landau orbital  $n$  experiences not only the external field  $E(t)$ , but also an internal one, the “molecular” field associated with  $e$ - $h$  pairs in Landau orbitals  $n'$ . For each  $n$ , external and Coulomb fields combine to give an effective self-consistent “local” field to which the system responds. The problem is thus similar to that of a paramagnet in an external magnetic field.

In order to describe pump-probe experiments, we split the laser field into two parts, a strong pump field  $E(t)$  propagating in the direction  $\mathbf{k}_2$  and a weak probe field  $\delta E(t)$  propagating in the direction  $\mathbf{k}_1$ . The former gives rise to a renormalized semiconductor “ground state,” described by Eqs. (6)–(9), while the linear response to the latter yields the corresponding renormalized “excitation spectrum.” Linearizing Eqs. (6)–(9) with respect to

$\delta E(t)$ , we find<sup>21,22</sup>

$$\frac{\partial}{\partial t} \delta \hat{n}_n(t) = -i[\delta \hat{\epsilon}_n(t), \hat{n}_n(t)] - i[\hat{\epsilon}_n(t), \delta \hat{n}_n(t)] + \left. \frac{\partial}{\partial t} \delta \hat{n}_n(t) \right|_{\text{relax}}, \quad (12)$$

where

$$\delta \hat{\epsilon}_n(t) = \begin{pmatrix} 0 & -\mu \delta E(t) \\ -\mu^* \delta E^*(t) & 0 \end{pmatrix} - \sum_{n'} V_{n,n'} \delta \hat{n}_{n'}(t). \quad (13)$$

The total polarization induced by the probe field is

$$\delta P(t) = \frac{\lambda \mu^*}{2\pi} \sum_n \delta \psi_n(t). \quad (14)$$

In typical time-resolved pump-probe experiments, after

$$\left[ i \frac{\partial}{\partial t} + i\gamma_2 - \lambda(2n-1) \right] \delta \psi_n(t) + \sum_{n'} V_{n,n'} \delta \psi_{n'}(t) = -[1-2n_n(t)]\mu \delta E(t) + 2\delta n_n(t)\mu E(t) + 2 \sum_{n'} V_{n,n'} [n_n(t)\delta \psi_{n'}(t) - \delta \psi_n(t)n_{n'}(t) + \delta n_n(t)\psi_{n'}(t) - \psi_n(t)\delta n_{n'}(t)], \quad (17)$$

where

$$\frac{\partial}{\partial t} n_n(t) = \left[ \frac{\partial}{\partial t} + 2\gamma_2 \right] |\psi_n(t)|^2 - \gamma_1 n_n(t) \quad (18)$$

and

$$\frac{\partial}{\partial t} \delta n_n(t) = \left[ \frac{\partial}{\partial t} + 2\gamma_2 \right] \delta \psi_n(t) \Big|_{E=0} - \psi_n^*(t) - \gamma_1 \delta n_n(t) \quad (19)$$

Here,  $n_n = n_{cn} = 1 - n_{vn}$  is the  $e$ - $h$  distribution. Equations (16)–(19) are appropriate for Lorentzian line shapes and strong quantum confinement, where population dephasing is dominated by radiative decay.<sup>4,5,7,8</sup> As usual, in the absence of proper dephasing, we have  $\gamma_1 = 2\gamma_2$ .

Without the nonlinear corrections, Eqs. (16) and (17) correspond to inhomogeneous Wannier equations driven by the pump and probe fields  $E(t)$  and  $\delta E(t)$ , respectively. In this limit, they describe the linear optical response of an unperturbed exciton, discussed in the preceding section [Eqs. (3)–(5)]. The nonlinear corrections in Eq. (17) describe the effects on the exciton of the Pauli exclusion principle, through phase-space-filling, i.e., exciton-photon interaction [first two terms on the right-hand side of Eq. (17)] and exciton-exciton interaction [last term on the rhs of Eq. (17)]. Note that the  $n'=n$  contribution to the latter vanishes, reflecting the *local* charge neutrality in a given Landau orbital. Hence, only  $e$ - $h$  pairs in different Landau orbitals interact with each other. Any asymmetry in the  $e$  and  $h$  wave functions would of course modify this result.<sup>14</sup>

The nonlinear corrections may also be divided into ex-

passing the sample, the probe beam is sent through a monochromator and registered by a slow, time-integrating detector. In this situation, we may define an effective optical susceptibility through

$$\chi(\omega) = \frac{\delta P(\omega)}{\delta E(\omega)}, \quad (15)$$

where only that part of  $\delta P(\omega)$  that propagates in the probe beam direction  $\mathbf{k}_1$  is to be considered.

If we approximate the relaxation terms in Eqs. (6) and (12) by phenomenological transverse and longitudinal relaxation rates  $\gamma_2$  and  $\gamma_1$ , respectively, we find in leading order in the pump field or intensity<sup>21,22,28</sup>

$$\left[ i \frac{\partial}{\partial t} + i\gamma_2 - \lambda(2n-1) \right] \psi_n(t) + \sum_{n'} V_{n,n'} \psi_{n'}(t) = -\mu E(t) \quad (16)$$

and

citon Hartree (proportional to  $n_n$ ) and exciton Fock (proportional to  $\delta n_n$ ) terms. The former are due to the (incoherent) population induced by the pump, while the latter are due to the (coherent) population modulation induced by both the pump and the probe [i.e., they describe the scattering of the pump beam (i) off the grating created by interference with the probe, and (ii) into the direction  $\mathbf{k}_1$  of the probe]. As is well known from studies of two-level atoms,<sup>29–31</sup> in a time-resolved ultrashort optical-pulse pump-probe experiment, these two types of nonlinear corrections have a different temporal evolution. The former dominate at positive time delays, and the latter at negative time delays.

#### A. Continuous-wave excitation

It is instructive to study first the solution of Eqs. (15)–(19) for continuous-wave excitation well below the absorption edge and in the complete absence of dephasing, i.e.,  $\gamma_1 = 2\gamma_2 \rightarrow 0$ . As discussed in Refs. 21 and 22, we may then parametrize the nonlinear optical susceptibility (15) in the same fashion as the linear optical susceptibility (5), but with renormalized transition energies and oscillator strengths that describe the nonresonant excitonic ac Stark effect. Following its initial observation in 1986 by Mysyrowicz *et al.*<sup>32</sup> and Von Lehmen *et al.*,<sup>33</sup> the latter has attracted a lot of attention recently, both experimentally and theoretically. In particular, calculations based on the unrestricted HF theory have clearly demonstrated that, contrary to widespread belief, the nonresonant excitonic ac Stark effect in two and three dimensions can in general not be understood in terms of two-level or uncorrelated  $e$ - $h$  pair models, except for huge

detunings from the absorption edge, exceeding the 3D Rydberg by more than 1 order of magnitude.<sup>28,34-37</sup> It is then quite natural to ask whether these deviations due to Coulomb interaction become quenched with increasing quantum confinement, as suggested earlier in Ref. 4.

By expanding  $\psi_n$  and  $\delta\psi_n$  in terms of the unperturbed exciton wave functions  $\phi_\alpha(n)$ , discussed in the preceding section, it is straightforward to derive from Eqs. (14)–(19) the nonlinear exciton-photon (ex-ph) and exciton-exciton (ex-ex) corrections to the transition energies and oscillator strengths.<sup>21,22</sup> For a monochromatic pump beam  $E(t) = E_p \exp(-i\omega_p t)$ , these corrections may be conveniently expressed in terms of the Green's functions<sup>28,34</sup>

$$G_p(n) = \sum_\alpha \frac{\phi_\alpha(n) \sum_{n'} \phi_\alpha(n')}{E_\alpha - \omega_p} \quad (20)$$

and

$$G_\alpha(n) = \sum_{\beta \neq \alpha} \frac{\phi_\beta(n) \sum_{n'} \phi_\beta(n')}{E_\beta - E_\alpha}. \quad (21)$$

Parametrizing the results in terms of those for a two-level atom with level spacing  $E_{1s}$ , one finds for the change in

exciton energy

$$\delta E_\alpha = \frac{2|\mu E_p|^2}{E_{1s} - \omega_p} \sigma_\alpha \quad (22)$$

and for the relative change in exciton oscillator strength

$$\frac{\delta f_\alpha}{f_\alpha} = - \frac{2|\mu E_p|^2}{(E_{1s} - \omega_p)^2} \rho_\alpha, \quad (23)$$

where

$$\sigma_\alpha^{\text{ex-ph}} = (E_{1s} - \omega_p) \sum_n \phi_\alpha^2(n) G_p(n), \quad (24)$$

$$\sigma_\alpha^{\text{ex-ex}} = (E_{1s} - \omega_p) \sum_{n,n'} V_{n,n'} [\phi_\alpha(n) - \phi_\alpha(n')] \phi_\alpha(n') \times [G_p(n) - G_p(n')] G_p(n), \quad (25)$$

$$\rho_\alpha^{\text{ex-ph}} = \frac{(E_{1s} - \omega_p)^2}{\sum_n \phi_\alpha(n)} \sum_n \phi_\alpha(n) [G_p(n) + 2G_\alpha(n)] G_p(n) \quad (26)$$

and

$$\rho_\alpha^{\text{ex-ex}} = \frac{(E_{1s} - \omega_p)^2}{\sum_n \phi_\alpha(n)} \sum_{n,n'} V_{n,n'} \{ [\phi_\alpha(n) - \phi_\alpha(n')] G_\alpha(n') + [G_\alpha(n) - G_\alpha(n')] \phi_\alpha(n') \} [G_p(n) - G_p(n')] G_p(n). \quad (27)$$

$\sigma_\alpha$  and  $\rho_\alpha$  are functions of the pump detuning  $(\omega_p - E_{1s})/E_0$  and are displayed in Fig. 3 for  $\lambda=1$  and 16 and the 1s, 2s, and 3s exciton states. The dashed lines show the exciton-photon contributions, while the solid lines include the exciton-exciton contributions as well. The number of Landau orbitals used in the calculation was 1000.

Numerical results for  $\sigma_\alpha$  and  $\rho_\alpha$  in two dimensions have been reported by a number of groups.<sup>28,34-37</sup> The general observation has been that for large detunings  $\sigma_\alpha$  and  $\rho_\alpha$  are dominated by the exciton-photon interaction, while for small detunings the exciton-exciton interaction dominates  $\sigma_\alpha$ , due to the quadratic dependence on inverse detuning of the population (modulation) terms. Figure 3 shows that these results persist in the presence of a perpendicular magnetic field. However, on a detuning scale that remains finite as  $l \rightarrow 0$  the nature of the renormalizations changes considerably.

As for the relative change in exciton oscillator strength,  $\rho_\alpha$ , Coulomb corrections are completely quenched as  $l \rightarrow 0$ :  $\rho_{1s}$  approaches the two-level result  $\rho_{1s} = 1$ , while  $\rho_{2s}, \rho_{3s}$ , etc., tend to zero, as suggested earlier.<sup>4</sup> The exciton-photon contribution to the change in exciton energy,  $\sigma_\alpha^{\text{ex-ph}}$ , displays a similar behavior; however, the exciton-exciton contribution  $\sigma_\alpha^{\text{ex-ex}}$  is not quenched, but shows a decrease in magnitude ( $\sigma_{1s}^{\text{ex-ex}}$ ) and/or a remarkable change in sign ( $\sigma_{2s}^{\text{ex-ex}}, \sigma_{3s}^{\text{ex-ex}}$ , etc.) with increasing magnetic field.

While the scaling with magnetic field of the exciton-photon contributions may be easily understood in terms of the increasing detuning of excited exciton states, the

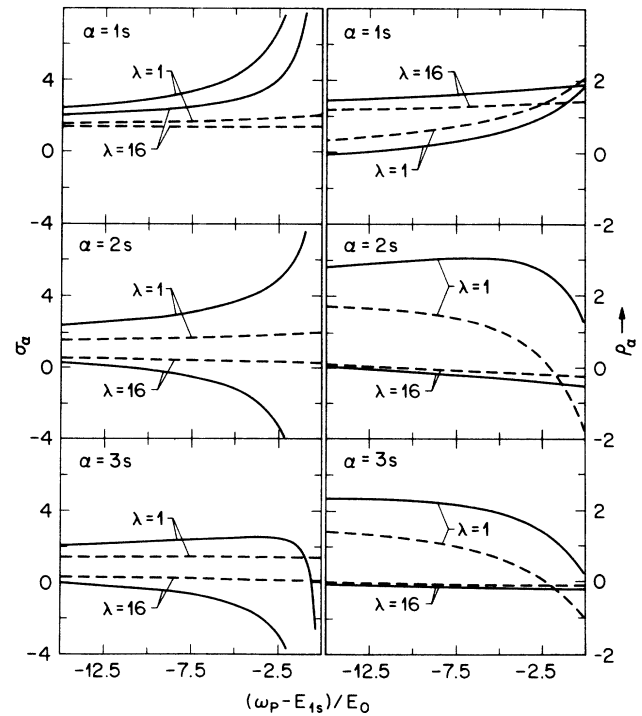


FIG. 3. Change in energy (relative change in oscillator strength) of the 1s, 2s, and 3s exciton states, normalized to that of a two-level atom  $2|\mu E_p|^2/(E_{1s} - \omega_p)$  [ $-2|\mu E_p|^2/(E_{1s} - \omega_p)^2$ ], vs pump detuning from the 1s exciton resonance  $(\omega_p - E_{1s})/E_0$  for  $\lambda=1$  and 16, calculated with a basis set of 1000 Landau orbitals. Solid lines: exciton-photon and exciton-exciton interaction. Dashed lines: exciton-photon interaction only.

behavior of the exciton-exciton contributions is more subtle, because several processes compete with each other. Consider the population (exciton Hartree) terms, for instance: vertex corrections renormalize the  $e$ - $h$  Coulomb interaction, decreasing the exciton binding energy and causing a blue shift, while self-energy corrections renormalize the individual  $e$  and  $h$  energies, decreasing the band gap and causing a red shift. As is well known, the extent to which these two effects cancel depends sensitively on the excitation conditions and the amount of  $e$ - $h$  correlation in the state under consideration.<sup>1,38</sup> (For example, for  $1s$  exciton excitation in two dimensions, self-energy corrections are important for all exciton states, while vertex corrections are most important for the  $1s$  ex-

citon state, giving rise to a pronounced net blue shift.<sup>1</sup>) The population modulation (exciton Fock) terms, on the other hand, yield a blue shift for all exciton states. For nonresonant excitation in zero magnetic field, all exciton states are blue shifted;<sup>28,34-37</sup> but as the magnetic field is increased, the excited exciton states behave more and more like uncorrelated  $e$ - $h$  pairs, so that their shift becomes dominated by ( $1s$  exciton) population-induced (inter-Landau-level) self-energy corrections. The  $1s$  exciton state, however, retains its correlated character up to the highest fields considered and hence always shows a blue shift, albeit of decreasing magnitude.

Consider now the third-order solution of Eqs. (14)–(19) for continuous-wave excitation and finite  $\gamma_1$  and  $\gamma_2$ ,

$$\chi^{(3)}(\omega) = -\frac{\lambda|\mu|^4}{\pi} \sum_n G(n) \left[ \frac{2\gamma_2}{\gamma_1} \left[ |G_p(n)|^2 + \sum_{n'} V_{n,n'} [ |G_p(n)|^2 G(n') - |G_p(n')|^2 G(n) ] \right] + \frac{\omega - \omega_p + i2\gamma_2}{\omega - \omega_p + i\gamma_1} \left[ G_p^*(n)G(n) + \sum_{n'} V_{n,n'} [ G_p^*(n)G_p(n')G(n) - G_p^*(n')G_p(n)G(n') ] \right] \right], \quad (28)$$

where we have introduced the Green's functions

$$G_p(n) = \sum_\alpha \frac{\phi_\alpha(n) \sum_{n'} \phi_\alpha(n')}{E_\alpha - \omega_p - i\gamma_2} \quad (29)$$

and

$$G(n) = \sum_\alpha \frac{\phi_\alpha(n) \sum_{n'} \phi_\alpha(n')}{E_\alpha - \omega - i\gamma_2}. \quad (30)$$

Figures 4–7 show the imaginary part of  $\chi^{(3)}(\omega)$ , i.e., the nonlinear absorption, for  $\lambda=1$  (Figs. 4 and 5) and 8 (Figs.

6 and 7) and various pump frequencies  $\omega_p$  (indicated by arrows), calculated with a basis set of 500 Landau orbitals.

For resonant  $1s$  exciton creation and excitation well below the absorption edge, Figs. 4 and 6 reiterate the physics discussed earlier. In these figures, the dephasing is entirely due to radiative decay, i.e.,  $\gamma_1=2\gamma_2$ . For intermediate magnetic fields,  $\lambda=1$ , the  $1s$ ,  $2s$ , and  $3s$  exciton states exhibit pronounced blue shifts due to the ac Stark effect [Fig. 4(a)]. Resonant  $1s$  exciton creation results in a blue shift and bleaching of the  $1s$  exciton state, similar to the behavior in zero magnetic field.<sup>1</sup> For excitation

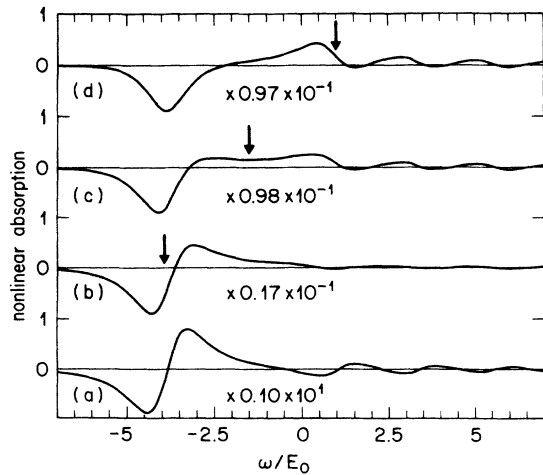


FIG. 4. Nonlinear absorption spectra for  $\lambda=1$ ,  $\gamma_1=2\gamma_2=2E_0$ , and various pump frequencies  $\omega_p$  (indicated by arrows), calculated with a basis set of 500 Landau orbitals. (a)  $\omega_p=E_{1s}-10E_0$ , (b)  $\omega_p=E_{1s}$ , (c)  $\omega_p=(E_{1s}+E_{2s})/2$ , (d)  $\omega_p=E_{2s}$ .

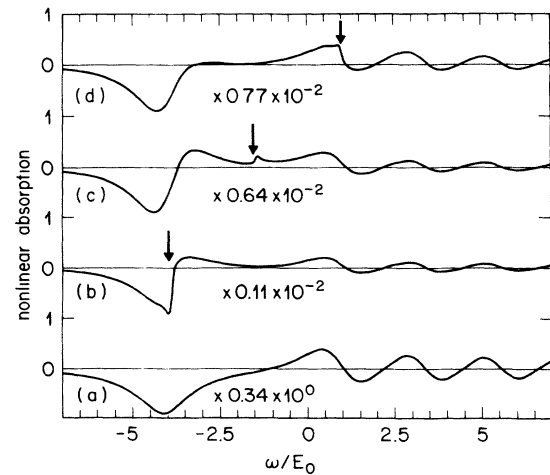


FIG. 5. Nonlinear absorption spectra for  $\lambda=1$ ,  $\gamma_1=0.1\gamma_2=0.1E_0$ , and various pump frequencies  $\omega_p$  (indicated by arrows), calculated with a basis set of 500 Landau orbitals. (a)  $\omega_p=E_{1s}-10E_0$ , (b)  $\omega_p=E_{1s}$ , (c)  $\omega_p=(E_{1s}+E_{2s})/2$ , (d)  $\omega_p=E_{2s}$ .

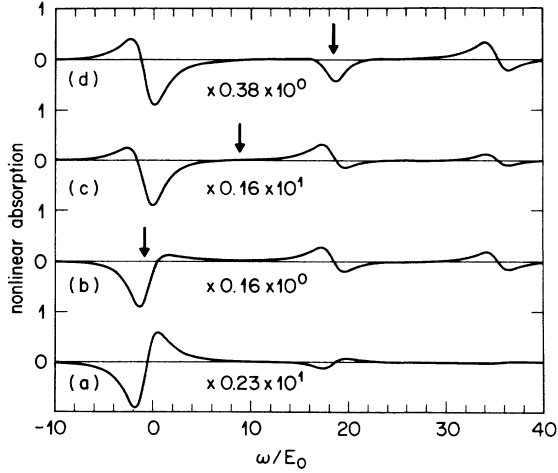


FIG. 6. Nonlinear absorption spectra for  $\lambda=8$ ,  $\gamma_1=2\gamma_2=4E_0$ , and various pump frequencies  $\omega_p$  (indicated by arrows), calculated with a basis set of 500 Landau orbitals. (a)  $\omega_p=E_{1s}-10E_0$ , (b)  $\omega_p=E_{1s}$ , (c)  $\omega_p=(E_{1s}+E_{2s})/2$ , (d)  $\omega_p=E_{2s}$ .

above the  $1s$  exciton resonance [Figs. 4(c) and 4(d)], the  $1s$  exciton state exhibits mainly a bleaching. For strong magnetic fields,  $\lambda=8$ , rather different behavior is obtained (Fig. 6). Resonant  $1s$  exciton creation [Fig. 6(b)] results now in pronounced red shifts of the  $2s$  and  $3s$  exciton states due to population-induced inter-Landau-level self-energy corrections, as explained earlier. Vice versa, the  $1s$  exciton state exhibits a pronounced red shift when  $2s$  excitons are excited [Fig. 6(d)]. These red shifts are the salient feature of the nonlinear optical response of 2D excitons in a strong perpendicular magnetic field.

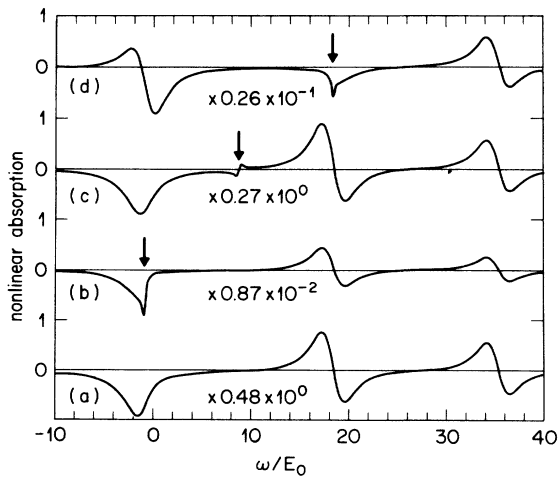


FIG. 7. Nonlinear absorption spectra for  $\lambda=8$ ,  $\gamma_1=0.1\gamma_2=0.2E_0$ , and various pump frequencies  $\omega_p$  (indicated by arrows), calculated with a basis set of 500 Landau orbitals. (a)  $\omega_p=E_{1s}-10E_0$ , (b)  $\omega_p=E_{1s}$ , (c)  $\omega_p=(E_{1s}+E_{2s})/2$ , (d)  $\omega_p=E_{2s}$ .

Figures 5 and 7 display the same quantities as Figs. 4 and 6, but with  $\gamma_1=0.1\gamma_2$ , so that there is a significant dephasing of the polarization beyond that induced by radiative decay, due for example to exciton-phonon interactions. As is well known from studies of two-level atoms,<sup>29</sup> such a proper dephasing has a dramatic influence on the nonlinear optical response. It reduces the contribution of the coherent population-modulation (exciton Fock) terms [second term on the rhs of Eq. (28)] compared to that of the incoherent population (exciton Hartree) ones [first term on the rhs of Eq. (28)], except for a narrow spectral region around the pump frequency, where the population can still follow the beat between pump and probe. This accounts for the small features in Figs. 5 and 7. Even for excitation well below the absorption edge and intermediate magnetic fields [Fig. 5(a)], the  $2s$  and  $3s$  exciton states now exhibit pronounced red shifts, due to the predominance of incoherent population effects. For the same reason, the ac Stark shift of the  $1s$  exciton state is replaced by a bleaching [Figs. 5(a) and 7(a)].

### B. Impulsive excitation

Recent advances in ultrashort optical-pulse techniques make it possible to excite several magnetoexciton states simultaneously, as has been done with vibronic states of organic dye molecules.<sup>39,40</sup> On general grounds, such impulsive excitation is expected to result in pronounced quantum beats in the time-resolved nonlinear optical response, due to the interference of polarization components oscillating with slightly different frequency. Below, we show that these quantum beats allow to resolve  $e-h$  cyclotron motion in real time.

First consider the limit of  $\delta$ -function pump and probe

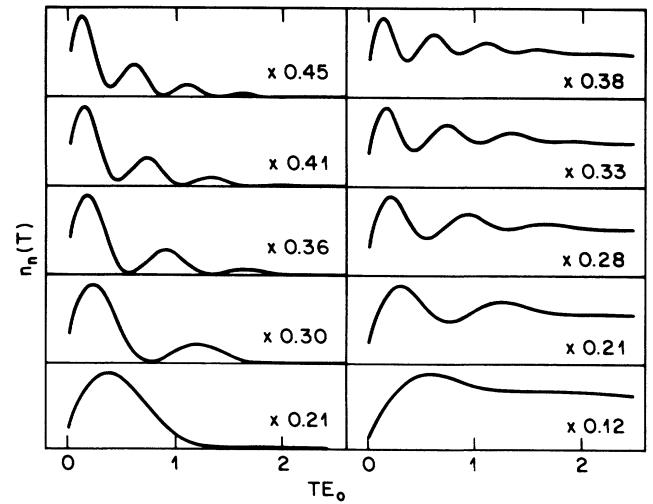


FIG. 8. Landau-level population  $n_1(T)$  (bottom) to  $n_5(T)$  (top) induced by a  $\delta$ -function pump pulse vs time delay  $T$  for  $\lambda=1$ ,  $\gamma_1=2\gamma_2=2E_0$  (left), and  $\gamma_1=0.1\gamma_2=0.1E_0$  (right), calculated with a basis set of 100 Landau orbitals.

pulses, such that all exciton states are excited simultaneously, since this is the easiest to calculate and already contains the interesting effects. When the pump precedes the probe, i.e., for positive time delays  $T$ , we obtain from Eqs. (14)–(19) the effective third-order susceptibility due to exciton-photon interaction,

$$\chi_{\text{ex-ph}}^{(3)}(\omega) = -\frac{\lambda|\mu|^2}{\pi|E_p|^2} \sum_n G(n)n_n(T), \quad T > 0 \quad (31)$$

where  $n_n(T)$  is the population induced in the  $n$ th Landau level by a pump pulse  $E(t) = E_p\delta(t)$ ,

$$n_n(T) = \Theta(T)|\mu E_p|^2 \sum_{\alpha\beta} \phi_\alpha(n) \sum_{n'} \phi_\alpha(n')\phi_\beta(n) \sum_{n''} \phi_\beta(n'') \frac{(E_\alpha - E_\beta)e^{i(E_\alpha - E_\beta)T - 2\gamma_2 T} + i(2\gamma_2 - \gamma_1)e^{-\gamma_1 T}}{E_\alpha - E_\beta + i(2\gamma_2 - \gamma_1)}. \quad (32)$$

For strong magnetic fields, all exciton states except for the  $1s$  are nearly diagonal in the Landau orbital basis. Then the population  $n_n(T)$  acquires an oscillatory modulation, the frequency of which varies approximately like  $n\omega_c$ , as shown in Figs. 8 and 9 for  $\lambda = 1$  and 8, respectively. (The number of Landau orbitals used in the calculation was 100.) This peculiar variety of quantum beats, wherein the population of a given exciton state oscillates approximately with the quantum number of that state, arises due to the  $\delta$ -function excitation and the Coulomb interaction, which provides the coupling necessary for interference. Without the latter, i.e., for  $\phi_\alpha(n) = \delta_{\alpha,n}$ , the population  $n_n(T)$  would simply decay like  $\exp(-i\gamma_1 T)$ .

Figures 10 show the imaginary part of  $\chi_{\text{ex-ph}}^{(3)}(\omega)$ , i.e., the time-resolved nonlinear absorption due to exciton-photon interaction, for  $\lambda = 8$  and positive time delays  $T$  between  $0.02E_0^{-1}$  (bottom) and  $0.34E_0^{-1}$  (top), calculated with a basis set of 20 Landau orbitals. The spectra display a bleaching of the  $1s$ ,  $2s$ , and  $3s$  exciton states that evolves in time similar to the respective populations  $n_n(T)$  and hence shows oscillations. These oscillations

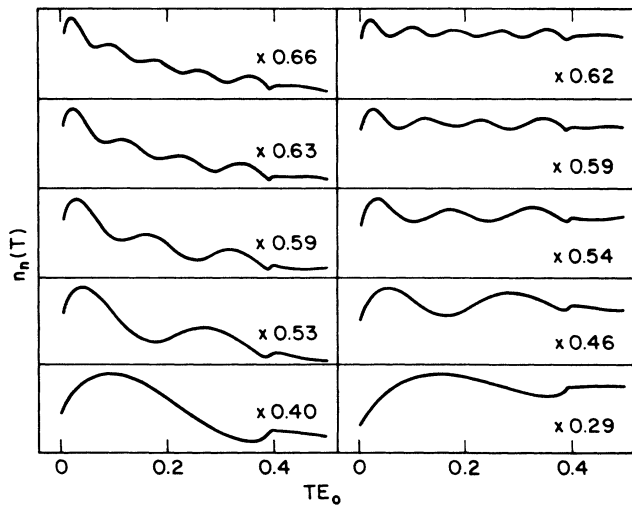


FIG. 9. Landau-level population  $n_1(T)$  (bottom) to  $n_5(T)$  (top) induced by a  $\delta$ -function pump pulse vs time delay  $T$  for  $\lambda = 8$ ,  $\gamma_1 = 2\gamma_2 = 4E_0$  (left), and  $\gamma_1 = 0.1\gamma_2 = 0.2E_0$  (right), calculated with a basis set of 100 Landau orbitals.

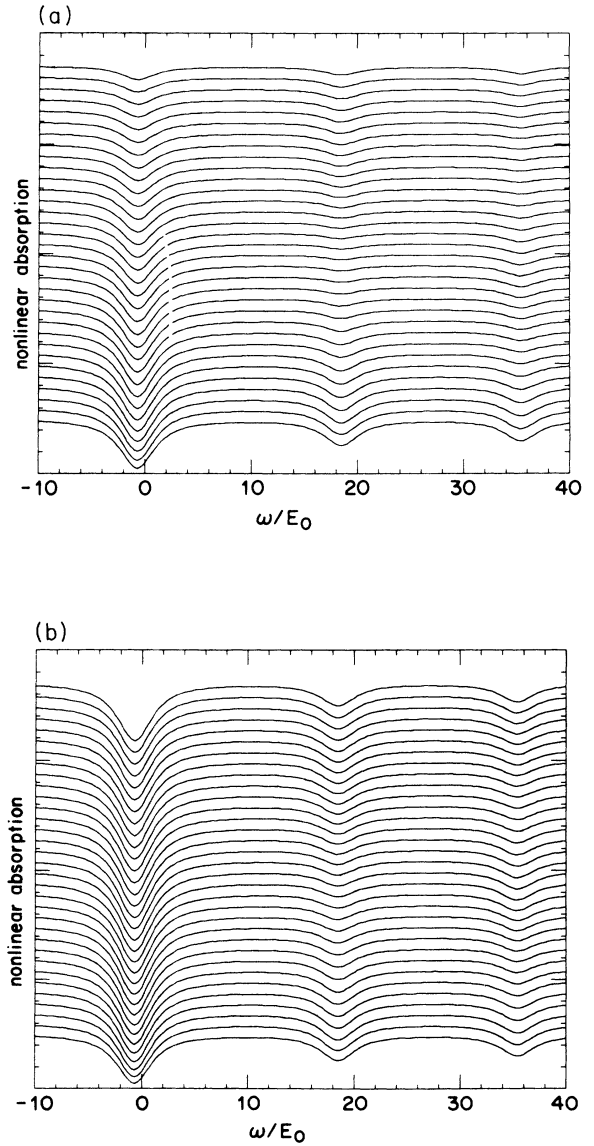


FIG. 10. Time-resolved nonlinear absorption spectra due to exciton-photon interaction for positive time delays  $T$  between  $0.02E_0^{-1}$  (bottom) and  $0.34E_0^{-1}$  (top),  $\lambda = 8$ , and  $\delta$ -function pump and probe pulses, calculated with a basis set of 20 Landau orbitals. (a)  $\gamma_1 = 2\gamma_2 = 4E_0$ , (b)  $\gamma_1 = 0.1\gamma_2 = 0.2E_0$ .

due to quantum beats should not be confused with the coherent oscillations that arise in ultrashort optical-pulse pump-probe experiments when the probe precedes the pump (see below).<sup>30,31,37,41,42</sup>

The exciton-exciton interaction yields an additional contribution to the effective third-order susceptibility  $\chi^{(3)}(\omega)$ . From Eqs. (14)–(19) we obtain for positive time delays  $T$

$$\chi_{\text{ex-ex}}^{(3)}(\omega) = \frac{\lambda|\mu|^4}{2\pi} \sum_{\alpha,\beta,\gamma,\delta} V_{\alpha,\beta,\gamma,\delta} \sum_n \phi_\alpha(n) \sum_{n'} \phi_\beta(n') \sum_{n''} \phi_\gamma(n'') \sum_{n'''} \phi_\delta(n''') \times \left[ \frac{(E_\beta - E_\gamma)(e^{i(E_\beta - E_\gamma)T - 2\gamma_2 T} + e^{i(E_\beta - E_\delta)T - 2\gamma_2 T})}{(E_\alpha - \omega - i\gamma_2)[E_\beta - E_\gamma + i(2\gamma_2 - \gamma_1)](\omega + E_\beta - E_\gamma - E_\delta + i3\gamma_2)} + \frac{i(2\gamma_2 - \gamma_1)(e^{i(E_\beta - E_\delta)T - 2\gamma_2 T} + e^{-\gamma_1 T})}{(E_\alpha - \omega - i\gamma_2)[E_\beta - E_\gamma + i(2\gamma_2 - \gamma_1)][\omega - E_\delta + i(\gamma_1 + \gamma_2)]} \right], \quad T > 0 \quad (33)$$

where

$$V_{\alpha,\beta,\gamma,\delta} = 2 \sum_{n,n'} V_{n,n'} \phi_\alpha(n) [\phi_\beta(n)\phi_\gamma(n')\phi_\delta(n') - \phi_\beta(n')\phi_\gamma(n)\phi_\delta(n)] \quad (34)$$

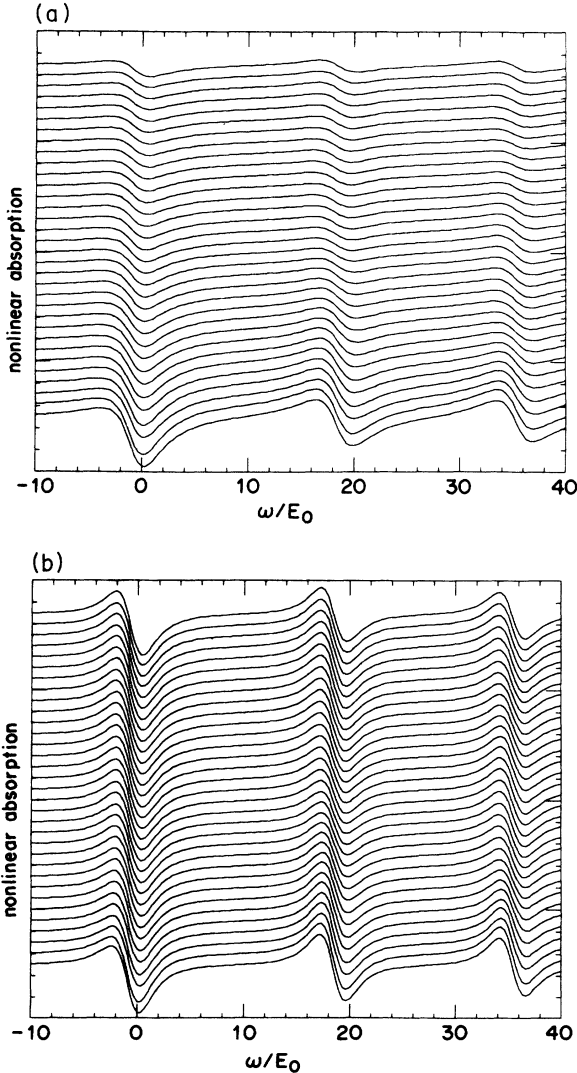


FIG. 11. Time-resolved nonlinear absorption spectra due to exciton-photon and exciton-exciton interaction for positive time delays  $T$  between  $0.02E_0^{-1}$  (bottom) and  $0.34E_0^{-1}$  (top),  $\lambda=8$ , and  $\delta$ -function pump and probe pulses, calculated with a basis set of 20 Landau orbitals. (a)  $\gamma_1=2\gamma_2=4E_0$ , (b)  $\gamma_1=0.1\gamma_2=0.2E_0$ .

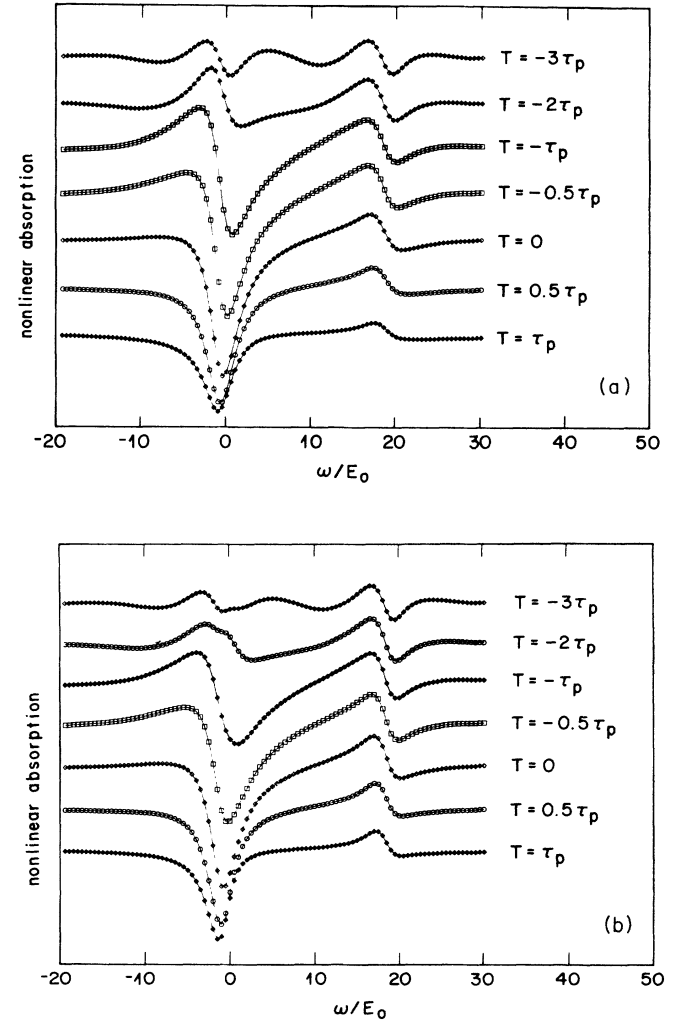


FIG. 12. Time-resolved nonlinear absorption spectra for various time delays  $T$ ,  $\lambda=8$ , and Gaussian pump and probe pulses of  $\tau_p=0.13E_0^{-1}$  duration centered in between the  $1s$  and  $2s$  exciton states, such that both states are excited simultaneously. The peak Rabi frequency of the pump pulse was  $|\mu E_p|=E_0$  and the spectra were calculated with a basis set of 100 Landau orbitals. (a)  $\gamma_1=2\gamma_2=4E_0$ , (b)  $\gamma_1=0.1\gamma_2=0.2E_0$ .

is the Heitler-London exchange integral.<sup>21,22,38</sup> Figure 11 shows the total time-resolved nonlinear absorption, i.e., the sum of the imaginary parts of  $\chi_{\text{ex-ph}}^{(3)}(\omega)$  and  $\chi_{\text{ex-ex}}^{(3)}(\omega)$ , for the same parameters as in Figs. 10. The spectra display a bleaching and red shifts of the 1s, 2s, and 3s exciton states, qualitatively similar to the continuous-wave results shown in Figs. 6 and 7, but with an oscillatory modulation of the decaying signal due to quantum beats.

Real experiments are performed with pulses of finite spectral width and, depending on the pump and probe conditions, are expected to yield results intermediate between those discussed above and those discussed in the preceding section. To this end, we have studied this question for  $\lambda=8$  and Gaussian pump and probe pulses of  $\tau_p=0.13E_0^{-1}$  duration centered in between the 1s and 2s exciton states, such that both states are excited simultaneously. For these realistic pulse profiles, it is advantageous to integrate directly (i.e., numerically) the full nonlinear equations (6)–(15), as has been done before in the context of the ac Stark effect in zero magnetic field.<sup>35,37</sup>

Figures 12 show the time-resolved nonlinear absorption in the spectral vicinity of the 1s and 2s exciton states for various time delays  $T$ , calculated with a basis set of 100 Landau orbitals for a peak Rabi frequency of the pump pulse equal to  $|\mu E_p|=E_0$ . For negative time delay  $T=-3\tau_p$ , the nonlinear absorption spectrum displays coherent oscillations that evolve continuously into a spectrum characteristic of 1s exciton bleaching and 2s exciton red shift at  $T=\tau_p$ , qualitatively similar to the corresponding continuous-wave results, Figs. 6(c) and 7(c). Comparison of Figs. 12(a) ( $\gamma_1=2\gamma_2$ ) and 12(b) ( $\gamma_1=0.1\gamma_2$ ) shows that for these time delays most of the

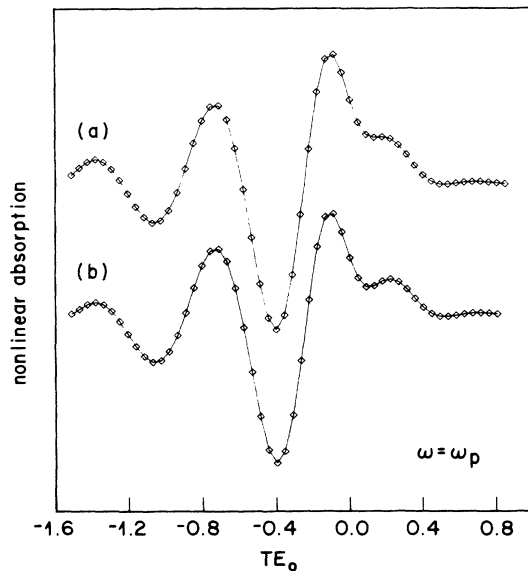


FIG. 13. Nonlinear absorption signal at the pump frequency  $\omega_p$  vs time delay  $T$  for  $\lambda=8$  and Gaussian pump and probe pulses of  $\tau_p=0.13E_0^{-1}$  duration centered in between the 1s and 2s exciton states, such that both states are excited simultaneously. The peak Rabi frequency of the pump pulse was  $|\mu E_p|=3E_0$  and the signal was calculated with a basis set of 100 Landau orbitals. (a)  $\gamma_1=2\gamma_2=4E_0$ , (b)  $\gamma_1=0.1\gamma_2=0.2E_0$ .

signal is coherent.

Figure 13 shows the nonlinear absorption signal at the pump frequency  $\omega_p$  versus time delay  $T$ , calculated with a basis set of 100 Landau orbitals for a peak Rabi frequency of the pump pulse equal to  $|\mu E_p|=3E_0$ . Two kinds of temporal oscillations are seen: when the probe precedes the pump, i.e., for negative time delays  $T$ , the signal displays coherent oscillations with a frequency  $\sim\omega_c/2$  determined by the probe detuning from resonance;<sup>30,31,37,41,42</sup> if on the other hand, the pump precedes the probe, i.e., for positive time delays  $T$ , the signal displays quantum beats with a frequency  $\sim\omega_c$  determined by the splitting of the 1s and 2s exciton states and due to their simultaneous excitation. As in Fig. 12, the bulk of the signal is again rather insensitive to the value of  $\gamma_1$ .

An alternative way to resolve  $e-h$  cyclotron motion in real time is to measure the signal generated by diffraction of the pump (i) off the grating created by interference with the probe, and (ii) into the direction  $2\mathbf{k}_2-\mathbf{k}_1$ . Such two-pulse self-diffraction experiments are often employed to study the temporal decay of the polarization due to dephasing processes.<sup>43</sup> For ultrashort optical pulses, the two-level theory of Yajima and Taira predicts that (in a homogeneously broadened system and with our definition of  $T$ ) the time-integrated signal rises as  $\exp(2\gamma_2 T)$  for negative time delays  $T$  and is zero otherwise.<sup>44</sup> Application of this theory to excitons has recently been criticized, because the internal exciton structure is completely ignored.<sup>45</sup>

We have evaluated the time-integrated two-pulse self-diffraction signal from Eqs. (6)–(14), by considering that part of  $\delta P(t)$  that propagates in the direction  $2\mathbf{k}_2-\mathbf{k}_1$ . Figure 14 shows the results for the same parameters as in

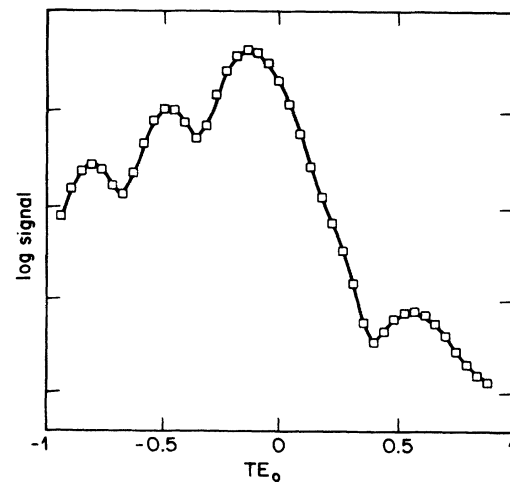


FIG. 14. Time-integrated two-pulse self-diffraction signal for  $\lambda=8$ ,  $\gamma_1=2\gamma_2=4E_0$ , and Gaussian pump and probe pulses of  $\tau_p=0.13E_0^{-1}$  duration centered in between the 1s and 2s exciton states, such that both states are excited simultaneously. The peak Rabi frequency of the pump pulse was  $|\mu E_p|=3E_0$  and the signal was calculated with a basis set of 50 Landau orbitals. No essential difference arises for  $\gamma_1=0.1\gamma_2=0.2E_0$ .

Fig. 13, calculated with a basis set of 50 Landau orbitals. Due to the simultaneous excitation of the  $1s$  and  $2s$  exciton states and their subsequent interference, the signal displays pronounced quantum beats (approximately) with the  $e$ - $h$  cyclotron frequency  $\omega_c$ . For negative time delays  $T$  its envelope rises as  $\exp(2\gamma_2 T)$ , as expected, while for positive time delays  $T$  an  $\exp(-4\gamma_2 T)$  decay is found. The latter feature is due to the exciton-exciton interaction and presents a novel effect which also exists in zero-magnetic field.

#### IV. CONCLUSIONS

We have studied the nonlinear optical response of spin-polarized two-dimensional excitons in a perpendicular magnetic field using the unrestricted Hartree-Fock approximation introduced earlier to account for electron-hole pairing correlations. This BCS-like theory becomes exact in the strong-field limit and can be readily extended to describe real quantum-well excitons. Our model should suffice as a first approximation that captures the essential physics of a more realistic treatment.

Contrary to the expectation that interaction effects become rapidly quenched with increasing magnetic field, i.e., quantum confinement, we find that inter Landau-level Coulomb correlations generally persist, giving rise to pronounced many-body effects in the nonlinear optical response. Qualitatively, this result is consistent with re-

cent theoretical studies of modulation-doped semiconductor heterostructures in perpendicular magnetic fields<sup>46,47</sup> and of semiconductor microcrystallites which also exhibit a quasi-zero-dimensional spectrum.<sup>8</sup> Thus, behavior indicative of noninteracting two-level systems is, strictly speaking, not recovered for finite magnetic fields. For excitation above the absorption edge and strong magnetic fields, the nonlinear absorption becomes dominated by bleaching and red shifts of the exciton states. Proper dephasing, for instance due to phonons, further increases the predominance of these effects.

The cyclotron motion of electron-hole pairs can be resolved in the time domain by use of ultrashort optical pulses that span several magnetoexciton states. Pronounced quantum beats are found both in nonlinear absorption and in two-pulse self-diffraction. These effects should be readily observable in GaAs or  $\text{In}_x\text{Ga}_{1-x}\text{As}$ -based quantum-well structures and we hope that our work will stimulate corresponding experiments.

During completion of this manuscript, we learned that results for the nonresonant excitonic ac Stark effect similar to ours have been obtained recently by Bauer.<sup>48</sup>

#### ACKNOWLEDGMENTS

We would like to thank Phil Becker, Daniel Chemla, Wayne Knox, Jason Stark, and Roland Zimmermann for several stimulating and useful discussions.

\*Permanent address: Physics Department, Princeton University, Princeton, NJ 08544.

<sup>1</sup>For a recent review, see S. Schmitt-Rink, D. S. Chemla, and D. A. B. Miller, *Adv. Phys.* **38**, 89 (1989).

<sup>2</sup>A. L. Efros and A. L. Efros, *Fiz. Tekh. Poluprovodn.* **16**, 1209 (1982) [*Sov. Phys.—Semicond.* **16**, 772 (1982)].

<sup>3</sup>L. E. Brus, *IEEE J. Quantum Electron.* **QE-22**, 1909 (1986).

<sup>4</sup>S. Schmitt-Rink, D. A. B. Miller, and D. S. Chemla, *Phys. Rev. B* **35**, 8113 (1987).

<sup>5</sup>E. Hanamura, *Phys. Rev. B* **37**, 1273 (1988).

<sup>6</sup>Yu. V. Vandyshev, V. S. Dneprovskii, A. I. Ekimov, D. K. Okorokov, L. B. Popova, and A. L. Efros, *Pis'ma Zh. Eksp. Teor. Fiz.* **46**, 393 (1987) [*JETP Lett.* **46**, 495 (1987)].

<sup>7</sup>L. Banyai, Y. Z. Hu, M. Lindberg, and S. W. Koch, *Phys. Rev. B* **38**, 8142 (1988).

<sup>8</sup>Y. Z. Hu, M. Lindberg, and S. W. Koch, *Phys. Rev. B* (to be published).

<sup>9</sup>F. C. Spano and S. Mukamel, *Phys. Rev. A* **40**, 5783 (1989).

<sup>10</sup>O. Akimoto and H. Hasegawa, *J. Phys. Soc. Jpn.* **22**, 181 (1967).

<sup>11</sup>M. Shinada and K. Tanaka, *J. Phys. Soc. Jpn.* **29**, 1258 (1970).

<sup>12</sup>A. H. MacDonald and D. S. Richie, *Phys. Rev. B* **33**, 8336 (1986).

<sup>13</sup>I. V. Lerner and Yu. E. Lozovik, *Zh. Eksp. Teor. Fiz.* **80**, 1488 (1981) [*Sov. Phys.—JETP* **53**, 763 (1981)].

<sup>14</sup>D. Paquet, T. M. Rice, and K. Ueda, *Phys. Rev. B* **32**, 5208 (1985).

<sup>15</sup>C. Kallin and B. I. Halperin, *Phys. Rev. B* **30**, 5655 (1984).

<sup>16</sup>A. H. MacDonald, *J. Phys. C* **18**, 1003 (1985).

<sup>17</sup>S. R. E. Yang and L. J. Sham, *Phys. Rev. Lett.* **58**, 2598

(1987).

<sup>18</sup>M. Shinada and S. Sugano, *J. Phys. Soc. Jpn.* **21**, 1936 (1966).

<sup>19</sup>G. W. Bryant, *Surf. Sci.* **196**, 596 (1988).

<sup>20</sup>G. W. Bryant, *Phys. Rev. Lett.* **59**, 1140 (1987).

<sup>21</sup>S. Schmitt-Rink and D. S. Chemla, *Phys. Rev. Lett.* **57**, 2752 (1986).

<sup>22</sup>S. Schmitt-Rink, D. S. Chemla, and H. Haug, *Phys. Rev. B* **37**, 941 (1988).

<sup>23</sup>E. Heiner, *Phys. Status Solidi B* **146**, 655 (1988).

<sup>24</sup>A. Stahl, *Z. Phys. B* **72**, 371 (1988).

<sup>25</sup>M. Lindberg and S. W. Koch, *Phys. Rev. B* **38**, 3342 (1988).

<sup>26</sup>P. W. Anderson, *Phys. Rev.* **112**, 1900 (1958).

<sup>27</sup>L. Banyai, *Phys. Rev. B* **39**, 8022 (1989).

<sup>28</sup>R. Zimmermann and M. Hartmann, *Phys. Status Solidi B* **150**, 365 (1988).

<sup>29</sup>R. W. Boyd and S. Mukamel, *Phys. Rev. A* **29**, 1973 (1984).

<sup>30</sup>C. H. Brito Cruz, J. P. Gordon, P. C. Becker, R. L. Fork, and C. V. Shank, *IEEE J. Quantum Electron.* **24**, 261 (1988).

<sup>31</sup>M. Lindberg and S. W. Koch, *Phys. Rev. B* **38**, 7607 (1988).

<sup>32</sup>A. Mysyrowicz, D. Hulin, A. Antonetti, A. Migus, W. T. Masselink, and H. Morkoç, *Phys. Rev. Lett.* **56**, 2748 (1986).

<sup>33</sup>A. Von Lehmen, D. S. Chemla, J. E. Zucker, and J. P. Heritage, *Opt. Lett.* **11**, 609 (1986).

<sup>34</sup>R. Zimmermann, *Phys. Status Solidi B* **146**, 545 (1988).

<sup>35</sup>W. Schaefer, *Adv. Solid State Phys.* **28**, 63 (1988).

<sup>36</sup>C. Ell, J. F. Mueller, K. El Sayed, and H. Haug, *Phys. Rev. Lett.* **62**, 304 (1989).

<sup>37</sup>I. Balslev, R. Zimmermann, and A. Stahl, *Phys. Rev. B* **40**, 4095 (1989).

<sup>38</sup>H. Haug and S. Schmitt-Rink, *Prog. Quantum Electron.* **9**, 3

- (1984).
- <sup>39</sup>H. L. Fragnito, J. Y. Bigot, P. C. Becker, and C. V. Shank, *Chem. Phys. Lett.* **160**, 101 (1989).
- <sup>40</sup>P. C. Becker, H. L. Fragnito, J. Y. Bigot, C. H. Brito Cruz, R. L. Fork, and C. V. Shank, *Phys. Rev. Lett.* **63**, 505 (1989).
- <sup>41</sup>B. Fluegel, N. Peyghambarian, G. Olbright, M. Lindberg, S. W. Koch, M. Joffre, D. Hulin, A. Migus, and A. Antonetti, *Phys. Rev. Lett.* **59**, 2588 (1987).
- <sup>42</sup>W. H. Knox, D. S. Chemla, D. A. B. Miller, J. B. Stark, and S. Schmitt-Rink, *Phys. Rev. Lett.* **62**, 1189 (1989).
- <sup>43</sup>L. Schultheis, J. Kuhl, A. Honold, and C. W. Tu, *Phys. Rev. Lett.* **57**, 1635 (1986).
- <sup>44</sup>T. Yajima and Y. Taira, *J. Phys. Soc. Jpn.* **47**, 1620 (1979).
- <sup>45</sup>I. Abram, *Phys. Rev. B* **40**, 5460 (1989).
- <sup>46</sup>S. Katayama and T. Ando, *Solid State Commun.* **70**, 97 (1989).
- <sup>47</sup>T. Uenoyama and L. J. Sham, *Phys. Rev. B* **39**, 11 044 (1989).
- <sup>48</sup>G. E. W. Bauer, *Phys. Rev. Lett.* **64**, 60 (1990).